A Lagrangian view of moisture transport related to the heavy rainfall of July 2020 in Japan: Importance of the moistening over the subtropical regions

N. Zhao[1], A. Manda[2], X. Guo[3], K. Kikuchi[3], T. Nasuno[1], M. Nakano[1], Y. Zhang[4], B. Wang[5]

[1] Research Institute for Global Change, Japan Agency for Marine-Earth Science and Technology, Yokosuka, 2370061, Japan.

[2] Earth and Environmental Sciences Division, Graduate School of Bioresources, Mie University, Mie, 5148507, Japan.

[3] International Pacific Research Center, School of Ocean and Earth Science and Technology, University of Hawaii, Honolulu, 96822, USA.

[4] Graduate School of Marine Science and Technology, Tokyo University of Marine Science and Technology, Tokyo, 1088477, Japan.

[5] College of Oceanography, Hohai University, Nanjing, 210098, China.

Corresponding author: Ning Zhao (zhaoning@jamstec.go.jp)

Key Points:

- Moisture came from both the tropical regions and subtropical regions
- The western Pacific Subtropical High is major forcing of moisture transport and also helped the moistening of low-level flows
- Subtropical regions (especially the western Pacific) contributed the most to the moisture accumulation

Abstract

The transport and accumulation of moisture played an essential role in the extremely heavy rainfall of July 2020 in Japan. To better understand this event in terms of moisture sources and transport routes, backward particle trajectory analysis was conducted. We found two major moisture sources: transport from the tropics and uptake from the subtropics. A narrow moisture channel was found along the edge of the western Pacific Subtropical High (WPSH), transporting the moisture to the Baiu front. However, most moisture from the tropics was lost due to precipitation, and their contributions were reduced to about 15%. In contrast, the subtropical regions contributed over 80% moisture via evaporation and lower tropospheric convection. Among those regions, the western Pacific contributed the most (33 %). This study highlights the role of WPSH in moisture transport, and also demonstrated the importance of the moisture uptake during the transport.

Plain Language Summary

Heavy rainfalls hit Japan in July 2020, and the related atmospheric river was found to be accumulated by the moisture from tropics and subtropics. The moisture was transported bya narrow moisture channel along the edge of western Pacific Subtropical High. But, due to the precipitation during the transport, the moisture from tropics decreased. On the other hand, when the air flows passed over the subtropical regions, they were moistened by evaporation and lower troposphere convection. Thus, our results suggest that the moisture from subtropical regions contributed the most in the moisture accumulation during the heavy rain event.

1 Introduction

Extremely heavy rain fell over Japan in July 2020 (hereafter, 20HR). The rainfall continued during this whole period and included several severe rainfall events. As reported by the Japan Meteorological Agency (JMA), during this event, the 48 hr precipitation exceeded 1300 mm in many regions of western Japan (e.g., Kyushu, Gifu, Kochi, and Nagano). Specifically, some records indicate that the total precipitation was equal to nearly half of the historical annual mean (e.g., Fukuoka, Kagoshima) (JMA, 2020). It was reported that 82 fatalities occurred, and 18,380 buildings were destroyed or damaged during the heavy rains (EOCJ, 2020).

Kamae (2020), based on a series of early analyses using the Japanese 55 year Reanalysis, showed that a narrow plume of water vapor transport (i.e., the atmospheric river, AR; also see Figure 1a) played a key role in the 20HR. According to the results in Kamae (2020) and JMA (2020), this AR started from the South China Sea (SCS) and passed through the southeast China mainland, before turning west along the Baiu front. It was also reinforced by the low level flows from the south, similar to the previous heavy rains in Japan (e.g., Shimpo et al., 2019;). Meanwhile, it is likely that the westward extension of the western Pacific Subtropical High (WPSH) also enhanced the northward moisture transport from the SCS to Japan (e.g., Naoi et al., 2020).

To date, the relationship between moisture transport and heavy rainfall during the Baiu season has been extensively studied (e.g., Zhou & Yu, 2005; Tsuji & Takayabu, 2019). Most studies have focused on the highly accumulated moisture itself (hence, the AR; e.g., Sampe & Xie, 2010; Guan & Waliser, 2019; Shimpo et al., 2019), but few of them paid attention to why such a massive amount of moisture accumulated and how was moisture transported (e.g., Bao et

al., 2006; Sodemenn & Stohl, 2013). As to the winter time ARs associated with extratropical cyclones, Bao et al. (2006) showed that the local moisture convergence associated with the warm conveyor belt (WCB) and cold fronts is the fundamental force of the cyclone related ARs, and they also uncovered the vigorous moisture gain/loss processes during the transport. Sodemann and Stohl (2013) further emphasized the essential role of the WCB airstream in the formation and maintenance of AR. However, even the strong convergence also occurred and helped the moisture accumulation near the Baiu front during the heavy rain (JMA, 2020), it remains unclear how moisture was transported to Japan, especially considering that the 20HR was preceded by the heavy rainfalls (hence, the great moisture loss) over southeastern China where the AR likely passed (e.g., Zhong, 2020, JMA 2020).

This study addresses two scientific topics: (1) the moisture sources of AR and transport routes and (2) moisture gain/loss processes along the routes. Since an Eulerian point of view has limitations to clarify the sources of moisture and the processes affecting moisture accumulation of AR (see Gimeno et al., 2012 and references therein), we performed a Lagrangian experiment based on backward trajectories, which have proven to be computationally efficient and useful in similar studies (e.g., Sodemann et al., 2008; Langhamer et al., 2018). We carried out a numerical hindcast to obtain high-resolution atmospheric fields for backward tracing and to evaluate the physical details. Due to the complexity of the multiple events during the 20HR, this study was based on one major precipitation event (3–4 July in Kyushu; hereafter 20HR1) that caused a flooding disaster (NHK World News, 2020).

This paper is organized as follows. Section 2 describes the numerical hindcast, backward trajectory experiment, and diagnostic variables for analyses. Subsections in Sec. 3 document the results, including the moisture sources, routes, and gain/loss processes during transport. The major findings are summarized in Sec. 4.

2 Materials and Methods

2.1 Numerical hindcast

To obtain high spatial and temporal resolution atmospheric fields for the backward trajectories, we performed a numerical hindcast based on the Weather Research and Forecasting model (WRF V4.1.5). Our model covered the East Aisan region (Figure 1), with 9-km mesh grids and 60 sigma layers from the surface to the top (50 hPa). The hindcast started from 27 June to 5 July. The boundary and initial conditions were interpolated from the 0.25-degree 6 hourly NCEP GDAS/FNL dataset (NCEP, 2015) and the sea surface temperature (SST) from the daily GHRSST MultiProduct Ensemble (Martin et al., 2012). The output was saved every 30 minutes, and the first day was for spin-up and not used. We use the WSM6 microphysics scheme (Hong & Lim, 2006), the Yonsei University PBL scheme (Hong et al., 2006), the Revised MM5 surface layer scheme (Jimenez et al., 2012), the United Noah Land Surface Model (Tewari et al., 2004), the RRTMG Shortwave and Longwave Schemes (Iacono et al., 2008), and the Grell–Freitas Ensemble cumulus scheme (Grell & Freitas, 2014).

To clearly represent the moisture transport and to validate the WRF output, we calculated the IVT that have been commonly used in previous studies (e.g., Lavers et al., 2012):

$$IVT = \sqrt{\left(\frac{1}{g}\int_{1000\ hPa}^{200\ hPa} qu\ dp\right)^2 + \left(\frac{1}{g}\int_{1000\ hPa}^{200\ hPa} qv\ dp\right)^2}, \quad (1)$$

where g is the gravitational acceleration, q is the specific humidity, p is the pressure, u and v are the zonal and the meridional wind, respectively.

We used the ERA5 reanalysis dataset (C3S, 2017) for model validation and comparison. As shown in Figure 1, our hindcast well reproduced the extremely high IVT, with strong water vapor fluxes from the surface to approximately 500 hPa. Our model showed good agreement with two satellite-based precipitation datasets in the localized heavy rain over the Kyushu (see Figure S1). Note that, although our model showed approximately 1 degree northward shift of the front and a lesser northward tilt with height (Figure 1), extra analyses demonstrated that the conclusions of this study were not sensitive to these mismatches and parameterizations we chose (see Text S1).

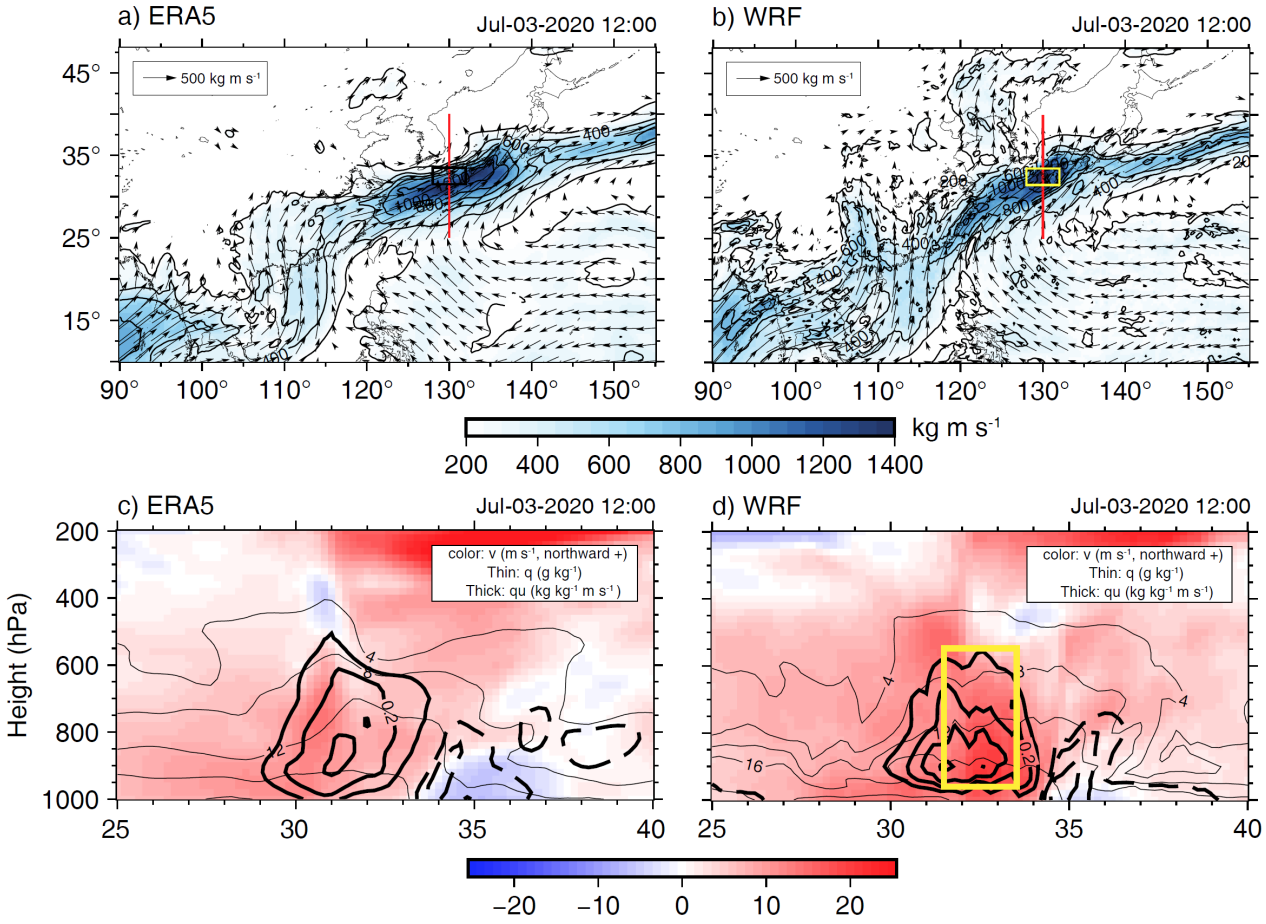

Figure 1. The vertically integrated water vapor transport (IVT, panels a and b) and vertical cross sections (panels c and d) along the 130 E on 3 July, 12 UTC based on ERA5 and WRF (FNL based). Yellow boxes show the region for particle releasing, and red lines in upper panels show the location of cross section.

2.2 Backward trajectories

To identify the moisture source and transport route, we applied a backward trajectory analysis of the passive particles based on the FLEXPART-WRF model (Version 3.3.2; Brioude et al., 2013), which has been widely used in studies on moisture transport (e.g., Langhamer et al.,

2018). We used the snapshot wind obtained from WRF and the Hanna scheme as recommended by Brioude et al. (2013) for the turbulence parameterization, with the convection scheme on.

Particles were released from 3rd July, 00 UTC to 4th July, 12 UTC during the 20HR1 with a 12 hr interval over Kyushu from the 950 hPa to the 550 hPa height level, where the strong water vapor fluxes located (129–132 E and 31.5–33.5 N; boxes in Figure 1). Each particle represented an air parcel with specific mass, and 10,000 particles (with total mass of 20 kg) were released in this study. All particles were backward traced to 28th June, and their locations and properties would not change again when they reached a boundary. Because this study focused on the moisture transport, we excluded particles originated north of 30 N, which are generally dry and cold particles. As a result, 8868 particles remained for further analyses.

2.3 Diagnostic variables

Changes in the moisture content of a specific particle *i* (ΔQ_i) predominantly reflect the effects of precipitation (p) and evaporation (e) processes (e.g., Stohl and James, 2004):

$$\Delta Q_{i,t} \approx Q_{i,t} - Q_{i,t-\Delta t} = \frac{m_{i,t}q_{i,t} - m_{i,t-\Delta t}q_{i,t-\Delta t}}{\Delta t} = e - p, \quad (2)$$

where $m_{i,t}$ is the mass of particle, $q_{i,t}$ is the specific humidity, t is time, Δt is the time interval (i.e., 30 mins), and $t = 0$ is the release time. For simplicity, the moisture uptake is regarded as $\Delta Q_{i,t} > 0$, and the precipitation is defined when $\Delta Q_{i,t} < 0$. Specifically, if moisture uptake occurred within the planetary boundary layer (PBL; obtained from WRF), a bulk evaporative moisture source (*E*) is identified, and we also adopted a factor of 1.5 to account for the potential underestimation and small scale variations of PBL.

To better evaluate the contribution of different moisture sources, we applied the 'source attribution' method as introduced by Sodemann et al. (2008). The general conception of this method is: a) once moisture uptake is detected, its weighted contribution would be determined ($f_{i,t} = \Delta Q_{i,t}/Q_{i,t}$), and all previous contributions wil be diluted; and b) if precipitation is detected, all previously gained moisture will be reduced according to the weighted contributions. In simple terms, moisture uptake at previous times would be 'filtered' by precipitation occurred later (i.e., 'rain-off'). Readers may refer to Text S2 for an example iteration for this method and Sodemann et al. (2008) for detailed descriptions.

The 'rain-off' filtered moisture uptake ($\Delta Q_{i,t,rain-off}$) for all particles in a specific atmospheric column yielded the final contribution for the accumulated moisture over the Kyushu region:

$$\Delta Q_{tot} \approx \frac{\sum_1^N (\Delta Q_{i,t,rain-off})}{A}. \quad (3)$$

where ΔQ_{tot} is the total 'rain-off' filtered moisture change, *N* is the total number of particles within the atmospheric column over a unit area *A* (0.5-degree mesh grid in this study). Similarly, moisture changes ($e - p$) for all particles in the column yielded the net surface freshwater flux (Romas et al., 2016):

$$E - P \approx \frac{\sum_1^N (e-p)}{A}, \quad (4)$$

where *E* is the evaporation rate, *P* is the precipitation rate.

3 Results

3.1 Moisture transport route

Figure 2a shows the horizontal trajectories of particles (i.e., air parcels). The air parcels of the 20HR1 mainly came from two tropical regions (Figure 1). Among the 8,868 particles, 6,380 (71.9%) of them came from the regions west of 122 E (the central longitude line of our domain), including the tropical Indian Ocean (IO) and the regions south of SCS, and 2,285 (25.8%) of particles came from the east (i.e., the tropical Pacific). The amount of water vapor carried by each particle from the west was lower than those particles from the east when they reached Kyushu (i.e., the release time). Moreover, our results also showed that all air parcels became moister during transport (Table S1).

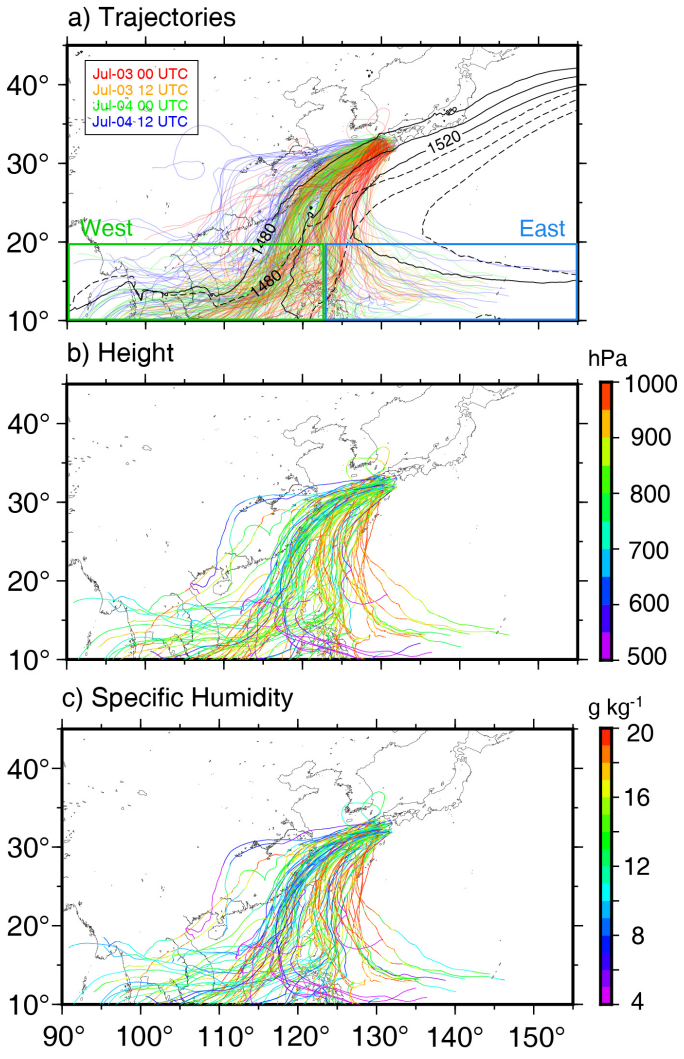

Figure 2. Trajectories of particles colored by the (a) released at different times, (b) pressure and (c) specific humidity. The mean 850 hPa (1480–1520 gpm) geopotential height are shown by

dashed (28th June–1st July) and solid lines (1st July–4th July). To avoid overcrowding, only one of every 100 trajectories was plotted.

The trajectories show that most particles travelled within mid-to-lower levels along the periphery of the WPSH, exhibiting a narrow moisture channel (i.e., the AR). This moisture channel varied from time to time, which is likely caused by the changing WPSH. For instance, particles released on 3rd July mainly passed over the East China Sea (ECS) (red curves in Figure 2a), while other trajectories shifted westward due to the westward extension of the WPSH in early July (see difference between the solid and dashed lines in Figure 2a). The particles travelling along the edge of WPSH distributed within the whole mid-to-lower troposphere (Figure 2b), while the particles in the east subducted and became moister simultaneous to the dominant WPSH (Figure 2c).

The moisture transport route of 20HR1 can be summarized as follows. In the first stage, the air parcels from the tropical IO were transported eastward (and/or northeastward) to the SCS, while other air parcels were transported westward from the tropical Pacific. After merging at approximately 20 N, the air parcels from these two tropical regions went farther north, guided by the WPSH, passing over southeastern China and the WP (and the marginal seas) in next few days. During the northward transport, some air parcels were subducted under the strengthening of WPSH. Within 1 or 2 days, the air parcels encountered the Baiu front at approximately 30 N and turned east along the front before reaching Japan. Readers may refer to an animation that shows the backward tracing of released particles (Video S1; see Data Availability section).

3.2 Moisture evolution during transport

To further understand the changes in moisture content shown in Figure 2, we examined the vertical distributions and moisture content of particles during transport. For simplicity, we consider the partiles in four layers: Lower (> 800 hPa), Mid-Lower (800–600 hPa), Mid (600–400 hPa), and Upper (< 400 hPa). As shown in Figure 3a, the variation trends of the particle numbers of Lower and Mid-Lower layers were quite different, although the numbers of particles were almost the same at both the release time and the end of tracing. More particles were subducted into the Lower layer, which facilitated gains of moisture from the sea surface. As a result, even we ignored the moisture gain-loss cycles, the net water vapor content of particles in the Lower layer increased about 20% during transport (dashed lines in Figure 3a). In contrast, while the particles kept entering the model domain, the particles in the Mid (Mid-Lower) layers decreased (changed only slightly) in numbers with slight change in moisture content, suggesting air parcels more likely subducted into lower levels, which is quite different from the results of ARs formed by WCB-like processes (Bao et al., 2006).

Figure 3b shows the time evolution of the ‘rain-off’ filtered moisture contributions of different regions. It is clear that the total moisture content continuously increased until the parcels reached Japan; however, the cause of this increase were different. During the first 2 days (day -5 and day -4), the increase was mainly due to the greater number of particles (hence, the air masses) that entering the domain, especially the low-level air flows(see the black lines in Figure 3a). In day -3, after the particles numbers reached its maximum, the amount of moisture from the tropics started decreasing due to the precipitation (the ‘rain-off’), and it declined almost linearly during the next two days. By contrast, more water vapor gained from the SCS and the WP, of which more than half was gained by the evaporation (see masked parts in Figure 3b). Especially, after day -1, the WP played the most important role in the moisture accumulation and finally

contributed 33.7% moisture at day 0 (i.e., release time). Note that the moisture contributed by the southeast China and the Baiu front was highly related to the heavy rainfalls there, which was likely caused by the re-evaporation of raindrops and the convective moistening (see the Subsection 3.3).

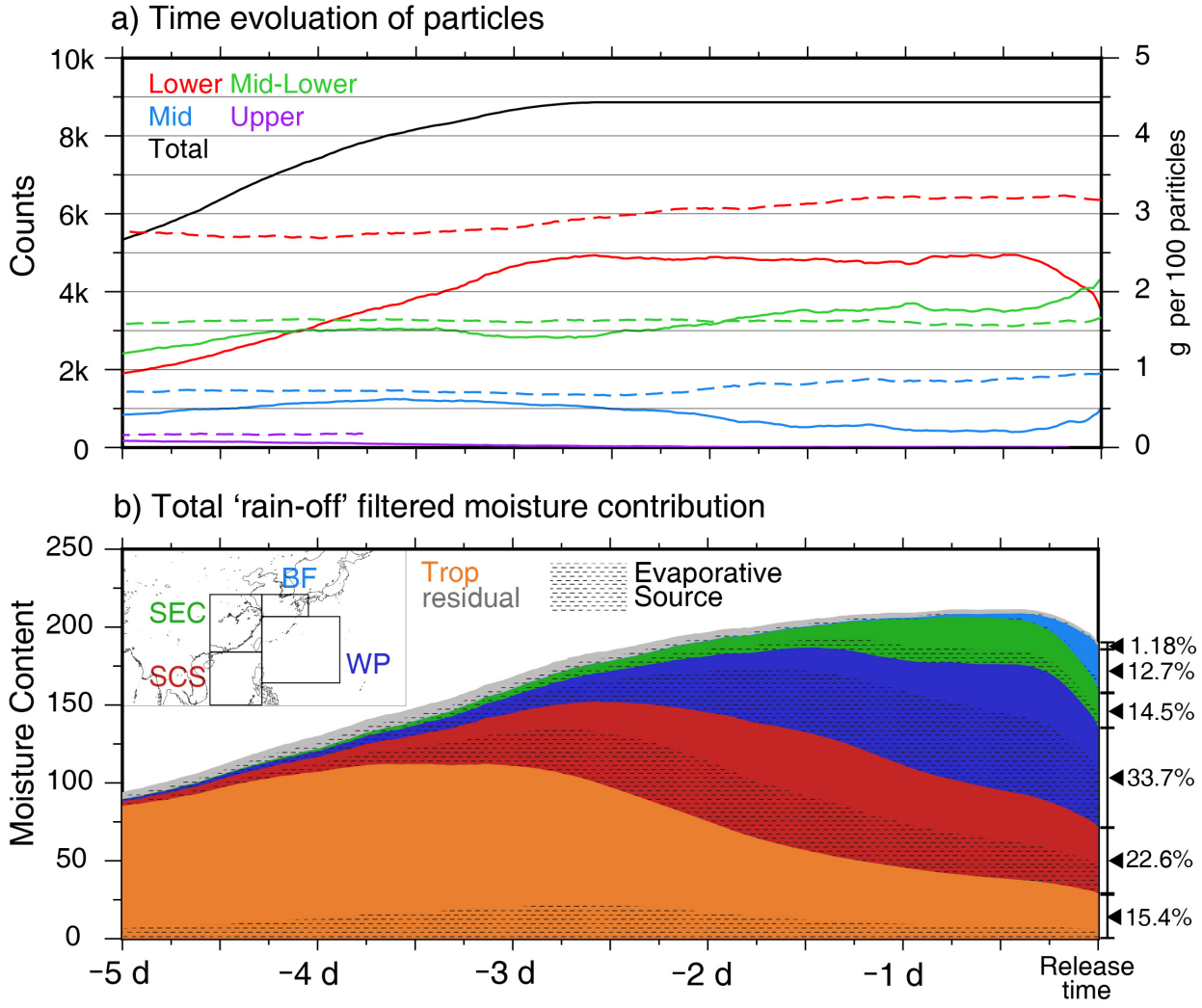

Figure 3. Composite time evolutions of (a) particle numbers (solid lines) and moisture (dashed lines; g per 100 particles) in different layers over the model domain, and (b) the total 'rain-off' filtered moisture contribution with their final fractions. Note that the 'Trop' includes the 'origin' moisture and moisture gained in tropical regions (south of 15 N, excluding the SCS).

To further show the horizontal distributions of moisture gain/loss processes along the transport, we evaluated the net surface freshwater fluxes (E-P). The strongest downward freshwater fluxes (hence, moisture loss) were found around 30 N, indicating heavy rainfall along the Baiu front (Figure 4a). Moreover, negative values were also found along the periphery of the WPSH and the coastal region where most of the Mid and Mid-Lower particles travelled (Figure 2b), suggesting that the moisture loss continued due to precipitaion along the transport routes. On the other hand, widely distributed positive freshwater fluxes over the SCS and the WP suggested the large amount of moisture was gained over those regions, which are consisting with the results of 'rain-off' filtered contributions (Figure 3b).

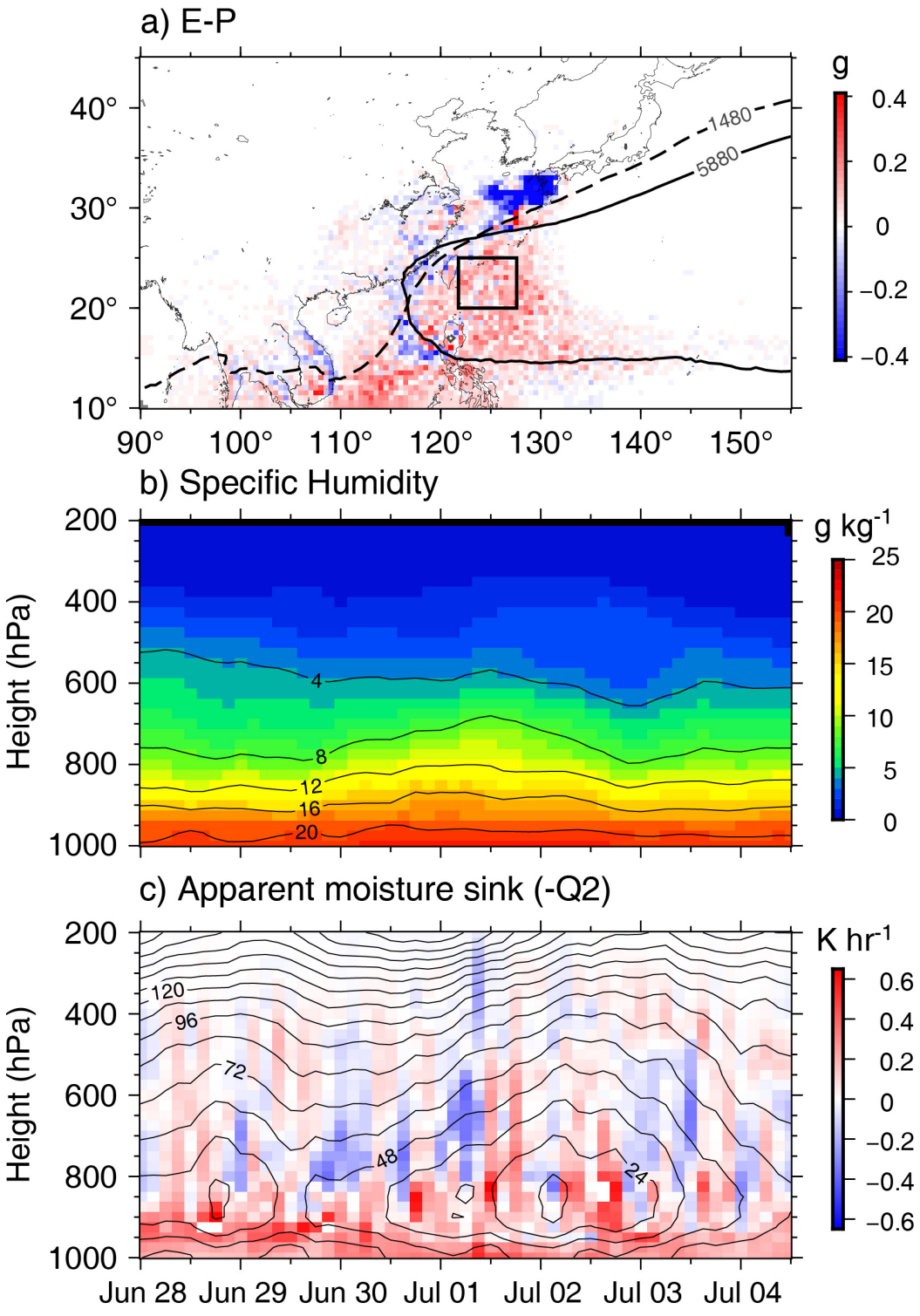

Figure 4. (a) The total net freshwater fluxes (E-P, upward positive), while contours show the WPSH by the mean geopotential height at 850 hPa (dashed) and 500 hPa (solid). (b) Time and height diagram of the area-averaged specific humidity and (c) apparent moisture sink (-*Q2*, positive means increase of moisture) with meridional geopotential height anomalies (contours) over the region (122.5–127.5 E, 20–25 N; black box in panel a).

3.3 Moistening processes

As shown in Figure 3b, about half of moisture was gained from non-evaporative sources over the subtropics. To reveal what processes helped such moistening, we examined the temporal variations in humidity and apparent moisture sink (*Q2*; e.g., Yanai et al., 1973; von Salzen et al., 2005) over the WP (see black box in Figure 4a). Figure 4b shows that rapid moistening occurred at lower levels from June 30th to July 3rd, when the top of the high humidity layer (> 8 g kg^{-1}) rose from 800 hPa to 700 hPa. The upward moisture transport showed good agreement with convection (see *-Q2* in Figure 4c; positive means moistening), exhibiting the environmental moistening by convection similar to that reported in tropical studies (e.g., Takemi, 2015). Although convection mostly remained shallow over this region due to the dominant WPSH (no clear precipitation, figure not shown), it facilitated lower troposphere moistening and boundary layer thickening.

It is now clear that the non-evaporative moistening over the WP was caused by the low-to-mid level convection along the moisture channel, and the moistened air parcels were then transported to Kyushu by low level flows and contributed to the moisture accumulation. Our analyses also shows that such high humidity low level flows may further enhance the quasi-stationary line shaped precipitation systems via the "back building" process and, therefore, the heavy rain in Kyushu (e.g., Schumacher & Johnson, 2005; Manda et al., 2014; See Text S3 for the analyses).

5 Conclusions

This study investigated the moisture sources and transport processes of the high accumulation of moisture associated with the heavy rains in July 2020, based on numerical hindcast and backward trajectory analyses. The 10000 particles with random masses were released from 3 July, 00:00 UTC to 4 July, 12:00 UTC, and 8,868 particles that originated south of 30 N were used for the analyses.

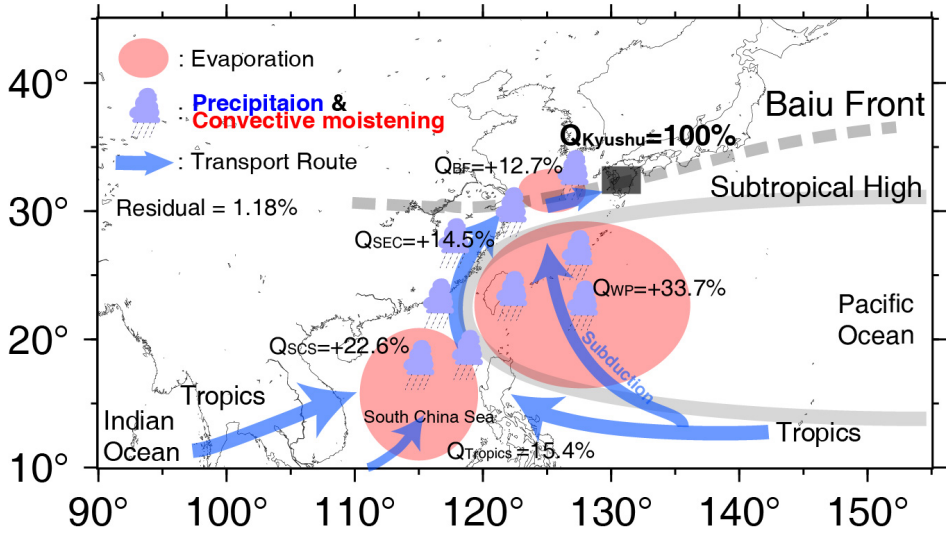

Figure 5. Schematic diagram for the transport route and contribution of the accumulated moisture during the 20HR1.

The backward trajectories exhibit a narrow moisture channel that started from the SCS at 20 N where most particles merged there. This channel was found to be located along the

periphery of the WPSH before encountering the Baiu front. Our finding about the moisture sources and transport are summarized schematically in Figure 5. There were two kinds of sources: (a) the moisture transported from tropical regions, including the IO, south of SCS and tropical Pacific, and (b) the moisture gained in subtropics during the transport. The moisture from tropical regions was continuously lost due to precipitation, resulting in a smaller contribution to the final moisture accumulation of 20HR1. Besides the evaporation, our analyses suggest that the air parcels acquired half of moisture via the lower tropospheric convection, especially over the WP where they subducted. Finally, the moisture from tropics (15%) and subtropics (85%) were accumulated as the form of AR along the Baiu front and contributed to the heavy rainfall in Kyushu.

The current study demonstrates that, rather than the moisture from the tropics, subtropical regions played the most important role in moisture accumulation and the heavy rain. Moreover, unlike the ARs that formed by the WCB-like ascending background airflows in the winter extratropical cyclones (e.g., Bao et al 2006; Sodemann & Stohl, 2013), the non-evaporative atmosphere moistening in subtropical regions was mainly induced by the self-constructed convection, even under the WPSH.

Although we revealed how was the moisture accumulated and transported to Japan, this study was mainly based on one major event during the heavy rains of July 2020; multi-casts and longer simulations could reduce the potential uncertainties. On the other hand, our study also suggests potential impacts of recent increasing sea surface temperatures over the subtropical WP (e.g., Bulgin et al. 2020) on the recorded heavy rainfall in Japan by enhancing the local evaporation and convection. These will be investigated as the next step of this study.

Acknowledgments

The authors are grateful to the quick analysis by Youichi Kamae (University of Tsukuba) and quick report by JMA on the 20HR. This work was partially supported by JSPS KAKENHI (JP19H05697 and JP17H02958) and the Collaborative Research Program (2020 S2-6) of RIAM, Kyushu University.

Data Availability

The data used in this study were listed with the website URL as follows: GSMaP (https://sharaku.eorc.jaxa.jp/GSMaP), GDAS/FNL (https://rda.ucar.edu/datasets/ds083.3), the ERA5 (https://cds.climate.copernicus.eu/), GMPE (http://marine.copernicus.eu), and TRMM (https://gpm.nasa.gov/data/directory). The trajectories used in this study and the trajectories animation are available on Zenodo.org (https://doi.org/10.5281/zenodo.3986631 and https://doi.org/10.5281/zenodo.4027542, respectively).

References

Bao, J.-W., Michelson, S. A., Neiman, P. J., Ralph, F. M., & Wilczak, J. M. (2006). Interpretation of enhanced integrated water vapor bands associated with extratropical cyclones: Their formation and connection to tropical moisture. *Monthly Weather Review*, 134, 1063–1080, https://doi.org/10.1175/MWR3123.1

315 Brioude, J., Arnold, D., Stohl, A., Cassiani, M., Morton, D., Seibert, P., et al. (2013). The
316 Lagrangian particle dispersion model FLEXPART-WRF version 3.1, *Geoscientific Model*
317 *Development*, 6, 1889–1904, doi:10.5194/gmd-6-1889-2013

318 Bulgin, C.E., Merchant, C.J. & Ferreira, D. (2020). Tendencies, variability and persistence of sea
319 surface temperature anomalies. *Scientific Reports*, 10, 7986, doi:10.1038/s41598-020-
320 64785-9

321 Copernicus Climate Change Service (C3S) (2017). ERA5: Fifth generation of ECMWF
322 atmospheric reanalyses of the global climate. Copernicus Climate Change Service
323 Climate Data Store (CDS), https://cds.climate.copernicus.eu, last accessed on 21 July
324 2020.

325 Emergency Operations Center of Japan (EOCJ) (2020). The damage situation during the heavy
326 rain of July 2020 (in Japanese), Report on 7 August 2020, EOCJ, available online:
327 www.bousai.go.jp/updates/r2_07ooame/pdf/r20703_ooame_33.pdf

328 Gimeno, L., Stohl, A., Trigo, R. M., Dominguez, F., Yoshimura, K., Yu, L., et al. (2012).
329 Oceanic and terrestrial sources of continental precipitation, *Reviews of Geophysics*, 50,
330 RG4003, doi:10.1029/2012RG000389

331 Grell, G. A., & Freitas, S. R. (2014). A scale and aerosol aware stochastic convective
332 parameterization for weather and air quality modeling, *Atmospheric Chemistry and*
333 *Physics*, 14, 5233–5250, doi:10.5194/acp-14-5233-2014

334 Guan, B., & Waliser, D. E. (2019). Tracking Atmospheric Rivers Globally: Spatial Distributions
335 and Temporal Evolution of Life Cycle Characteristics, *Journal of Geophysical Research:*
336 *Atmospheres*, 124, 12,523–12,552. https://doi.org/10.1029/2019JD031205

337 Hirota, N., Takayabu, Y. N., Kato, M., & Arakane, S. (2016). Roles of an Atmospheric River
338 and a Cutoff Low in the Extreme Precipitation Event in Hiroshima on 19 August 2014,
339 *Monthly Weather Review*, 144, 1145–1160, doi:10.1175/MWR-D-15-0299.1

340 Hong, S. Y., & Lim, J. O. J. (2006). The WRF single–moment 6–class microphysics scheme
341 (WSM6), *Journal of the Korean Meteorological Society*, 42, 129–151.

342 Hong, S. Y., Noh, Y., & Dudhia, J. (2006). A new vertical diffusion package with an explicit
343 treatment of entrainment processes, *Monthly Weather Review*, 134, 2318–2341,
344 doi:10.1175/MWR3199.1

345 Iacono, M. J., Delamere, J. S., Mlawer, E. J., Shephard, M. W., Clough, S. A., & Collins, W. D.
346 (2008). Radiative forcing by long–lived greenhouse gases: Calculations with the AER
347 radiative transfer models, *Journal of Geophysical Research*, 113, D13103,
348 doi:10.1029/2008JD009944

349 Japan Meteorological Agency (JMA) (2020). Characteristics of the heavy rain of July 2020 and
350 related atmospheric circulation (in Japanese), Press Release on 31 July 2020, JMA,
351 available online: www.jma.go.jp/jma/press/2007/31a/r02gou.pdf

352 Jimenez, P. A., Dudhia, J., Gonzalez–Rouco, J. F., Navarro J., Montavez, J. P., & Garcia–
353 Bustamante, E. (2012). A revised scheme for the WRF surface layer formulation,
354 *Monthly Weather Review*, 140, 898–918. doi:10.1175/MWR-D-11-00056.1

Kamae, Y. (@YKamae_JP) (2020). The heavy rain of July 2020, twitter.com/i/events/1280712104467550209, *Twitter*, last access: 13 September 2020.

Langhamer, L., Sauter, T., & Mayr, G. J. (2018). Lagrangian Detection of Moisture Sources for the Southern Patagonia Icefield (1979–2017), *Frontiers in Earth Science*, 6, 219, doi:10.3389/feart.2018.00219

Lavers, D. A., Villarini, G., Allan, R. P., Wood, E. F., & Wade, A. J. (2012). The detection of atmospheric rivers in atmospheric reanalyses and their links to British winter floods and the large-scale climatic circulation, *Journal of Geophysical Research*, 117, D20106, doi:10.1029/2012JD018027

Manda, A., Nakamura, H., Asano, N., Iizuka, S., Miyama, T., Moteki, Q., et al. (2014). Impacts of a warming marginal sea on torrential rainfall organized under the Asian summer monsoon, *Scientific Reports*, 4, DOI:10.1038/srep05741

Martin, M., Dash, P., Ignatov, A., Banzon, V., Beggs, H., Brasnett, B., et al. (2012). Group for High Resolution Sea Surface temperature (GHRSST) analysis fields inter-comparisons. Part 1: A GHRSST multi-product ensemble (GMPE), *Deep-Sea Research Part II*, 77-80, 21–30, doi:10.1016/j.dsr2.2012.04.013

Naoi, M., Kamae, Y., Ueda, H., & Mei, W. (2020). Impacts of seasonal transitions of ENSO on atmospheric river activity over East Asia, *Journal of the Meteorological Society of Japan*, 98, 655–668, doi:10.2151/jmsj.2020-027

NCEP/NWS/NOAA/U.S. Department of Commerce (2015). NCEP GDAS/FNL 0.25 Degree Global Tropospheric Analyses and Forecast Grids. Research Data Archive at the National Center for Atmospheric Research, Computational and Information Systems Laboratory, doi:10.5065/D65Q4T4Z. Last accessed on 21 July 2020.

Ramos, A. M., Nieto, R., Tomé, R., Gimeno, L., Trigo, R. M., Liberato, M. L. R., & Lavers, D. A. (2017). Atmospheric rivers moisture sources from a Lagrangian perspective, *Earth System Dynamics*, 7, 371–384, doi:10.5194/esd-7-371-2016

Sampe, T., & Xie, S. P. (2012). Large-scale dynamics of the Meiyu-Baiu rainband: Environmental forcing by the Westerly Jet, *Journal of Climate*, 23, 1, 113-134, doi:10.1175/2009JCLI3128.1

Schumacher, R. S., & Johnson, R. H. (2005). Organization and Environmental Properties of Extreme-Rain-Producing Mesoscale Convective Systems, *Monthly Weather Review*, 133, 961–976, doi:10.1175/MWR2899.1

Shimpo, A., Takemura, K., Wakamatsu, S., Togawa, H., Mochizuki, Y., Takekawa, M., et al. (2019). Primary Factors behind the Heavy Rain Event of July 2018 and the Subsequent Heat Wave in Japan, *Scientific Online Letters on the Atmosphere*, 15A, 13−18, doi:10.2151/sola.15A-003

Stohl, A., & James, P. (2004). A Lagrangian Analysis of the Atmospheric Branch of the Global Water Cycle. Part I: Method Description, Validation, and Demonstration for the August 2002 Flooding in Central Europe, *Journal of Hydrometeorology*, 5 (4), 656–678, doi:10.1175/1525-7541(2004)005<0656:ALAOTA>2.0.CO;2

Sodemann, H., Schwierz, C., & Wernli, H. (2008). Interannual variability of Greenland winter precipitation sources: Lagrangian moisture diagnostic and North Atlantic Oscillation influence, *Journal of Geophysical Research*, 113, D03107, doi:10.1029/2007JD008503

Sodemann, H., & A. Stohl, A. (2013). Moisture origin and meridional transport in atmospheric rivers and their association with multiple cyclones. *Monthly Weather Review*, 141, 2850-2868. https://doi.org/10.1175/MWR-D-12-00256.1

Takemi, T. (2015). Relationship between cumulus activity and environmental moisture during the CINDY2011/DYNAMO field experiment as revealed from convection-resolving simulations, *Journal of the Meteorological Society of Japan*, 93A, 41-58, doi:10.2151/jmsj.2015-035

Tewari., M., Chen, F., Wang, W., Dudhia, J., LeMone, M., Mitchell, K., et al. (2004). Implementation and verification of the unified Noah land surface model in the WRF model, 20th Conference on Weather Analysis and Forecasting/16th Conference on Numerical Weather Prediction. 11-15 January, 2004, Seattle, Washington.

Tsuguti, H., Seino, N., Kawase, H., Imada, Y., Nakaegawa, T., & Takayabu, I. (2019). Meteorological overview and mesoscale characteristics of the Heavy Rain Event of July 2018 in Japan, *Landslides*, 16, 363–371, doi:10.1007/s10346-018-1098-6, 2019

Tsuji, H., & Takayabu, Y. N. (2019). Precipitation Enhancement via the Interplay between Atmospheric Rivers and Cutoff Lows, *Monthly Weather Review*, 147, 2451–2466, doi:10.1175/MWR-D-18-0358.1

von Salzen, K., McFarlane, N. A., & Lazare, M. (2015). The role of shallow convection in the water and energy cycles of the atmosphere, *Climate Dynamics*, 25, 671–688, doi:10.1007/s00382-005-0051-2

NHK World News (2020). Kuma River overflow leads to extensive flooding., *NHK World News – At a Glance*, https://www3.nhk.or.jp/nhkworld/en/news/ataglance/1030/, last accessed: 13 September 2020.

Yanai, M., Esbensen, S., & Chu, J. H. (1973). Determination of bulk properties of tropical cloud clusters from large scale heat and moisture budgets, *Journal of the Atmospheric Sciences*, 30 (4), 611–627. doi: 10.1175/765 1520-0469(1973)030h0611:DOBPOTi2.0.CO;2

Zhong, R. (2020). Severe Floods in China Leave Over 106 Dead or Missing, *The New York Times*, https://www.nytimes.com/2020/07/03/world/asia/china-floods-rain.html, last access: 13 September 2020, 2020.

Zhou, T. J., & Yu, R. C. (2005). Atmospheric water vapor transport associated with typical anomalous summer rainfall patterns in China, *Journal of Geophysical Research*, 110, D08104, doi:10.1029/2004JD005413

References from the Supporting Information

Dudhia, J., (1989). Numerical study of convection observed during the Winter Monsoon Experiment using a mesoscale two–dimensional model. *Journal of the Atmospheric Sciences*, 46, 3077–3107. doi:10.1175/1520-0469(1989)046<3077:NSOCOD>2.0.CO;2

Huffman, G., Bolvin, D., Braithwaite, D., Hsu, K., Joyce, R., Xie, P. (2014). Integrated Multi-satellitE Retrievals for GPM (IMERG), version 4.4. NASA's Precipitation Processing Center, accessed 1st August, 2020, ftp://arthurhou.pps.eosdis.nasa.gov/gpmdata/

Kubota, T., Aonashi, K., Ushio, T., Shige, S., Takayabu, Y. N., Kachi, M., et al. (2020). Global Satellite Mapping of Precipitation (GSMaP) products in the GPM era. In V. Levizzani, C. Kidd, D. Kirschbaum, C. Kummerow, K. Nakamura, F. Turk (Eds.), *Satellite precipitation measurement* (Vol. 67, pp. 355–373), Switzerland, Springer, doi:10.1007/978-3-030-24568-9_20

Langhamer, L., Sauter, T., & Mayr, G. J. (2018). Lagrangian Detection of Moisture Sources for the Southern Patagonia Icefield (1979–2017), *Frontiers in Earth Science*, 6, 219, doi:10.3389/feart.2018.00219

Mlawer, E. J., Taubman, S. J., Brown, P. D., Iacono, M. J., & Clough, S. A. (1997). Radiative transfer for inhomogeneous atmospheres: RRTM, a validated correlated–k model for the longwave. *Journal of Geophysical Research*, 102, 16663–16682. doi:10.1029/97JD00237

Olson, J. B., Kenyon, J. S, Angevine, W. M., Brown, J. M., Pagowski, M., & Sušelj, K. (2019). A Description of the MYNN-EDMF Scheme and the Coupling to Other Components in WRF–ARW. *NOAA Technical Memorandum OAR GSD*, 61, 37, doi:10.25923/n9wm-be49

Schumacher, R. S., & Johnson, R. H. (2005). Organization and Environmental Properties of Extreme-Rain-Producing Mesoscale Convective Systems. *Monthly Weather Review*, 133, 961–976, https://doi.org/10.1175/MWR2899.1.

Shinoda, T., Uyeda, H., & Yoshimura, K. (2005). Structure of Moist Layer and Sources of Water over the Southern Region Far from the Meiyu/Baiu Front, *Journal of the Meteorological Society of Japan*, 83, 2, 137-152, doi:10.2151/jmsj.83.137

Sodemann, H., Schwierz, C., & Wernli, H. (2008). Interannual variability of Greenland winter precipitation sources: Lagrangian moisture diagnostic and North Atlantic Oscillation influence, *Journal of Geophysical Research*, 113, D03107, doi:10.1029/2007JD008503

Tao, W.-K., Wu, D., Lang, S., Chern, J.-D., Peters-Lidard, C., Fridlind, A., & Matsui, T. (2016). High-resolution NU-WRF simulations of a deep convective-precipitation system during MC3E: Further improvements and comparisons between Goddard microphysics schemes and obser- vations. *Journal of Geophysical Research*: *Atmospheres*, 121, 1278–1305. doi:10.1002/2015JD023986.

Tu, C. C., Chen, Y. L., Lin, P. L., & Lin, P. H. (2020). The relationship between the boundary layer moisture transport from the South China Sea and heavy rainfall over Taiwan, *Terrestrial Atmospheric and Oceanic Sciences*, 31, 159-176, doi: 10.3319/TAO.2019.07.01.01